ACS NANOSCIENCE Au
AN OPEN ACCESS JOURNAL OF THE AMERICAN CHEMICAL SOCIETY

pubs.acs.org/nanoau Article

Finite-Size Effects on Energy Transfer between Dopants in Nanocrystals

Mark J. J. Mangnus, Jeffrey Zom, Tom A. J. Welling, Andries Meijerink, and Freddy T. Rabouw*

Cite This: *ACS Nanosci. Au* 2022, 2, 111−118 Read Online

ACCESS | Metrics & More | Article Recommendations | Supporting Information

ABSTRACT: Many phosphor materials rely on energy transfer (ET) between optically active dopant ions. Typically, a donor species absorbs light of one color and transfers the energy to an acceptor species that emits light of a different color. For many applications, it is beneficial, or even crucial, that the phosphor is of nanocrystalline nature. Much unlike the widely recognized finite-size effects on the optical properties of quantum dots, the behavior of optically active ions is generally assumed to be independent of the size or shape of the optically inactive host material. Here, we demonstrate that ET between optically active dopants is also impacted by finite-size effects: Donor ions close to the surface of a nanocrystal (NC) are likely to have fewer acceptors in proximity compared to donors in a bulk-like coordination. As such, the rate and efficiency of ET in nanocrystalline phosphors are low in comparison to that of their bulk counterparts. Surprisingly, these undesired finite-size effects should be considered already for NCs with diameters as large as 12 nm. If we suppress radiative decay of the donor by embedding the NCs in media with low refractive indices, we can compensate for finite-size effects on the ET rate. Experimentally, we demonstrate these finite-size effects and how to compensate for them in YPO_4 NCs co-doped with Tb^{3+} and Yb^{3+}.

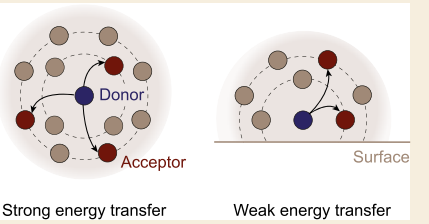

KEYWORDS: *energy transfer, lanthanide ions, nanocrystals, luminescence, Monte Carlo simulations, quantum cutting, finite-size effects*

INTRODUCTION

Phosphors convert the color of incident light. Generally, they are crystalline materials doped with optically active dopant ions, such as lanthanide ions. It may be advantageous to incorporate multiple species of dopant ions in the same material. In such a design, one species can have a strong absorption overlapping with the spectrum of incident photons, while a second species emits light of the desired color. To combine these two functionalities, energy transfer (ET) between the dopant species is crucial. ET between lanthanide ions via dipole−dipole interactions has been extensively studied in microcrystalline phosphors, and several mechanisms of ET have been identified.[1−6] However, certain applications, including nanothermometry,[7−9] bioimaging and cancer treatment,[10,11] and spectral conversion for photovoltaics,[12] require that the phosphor is a nanomaterial.

Photoluminescence (PL) from doped nanocrystals (NCs) is typically less efficient than that of microcrystalline phosphors, especially when their dimensions become increasingly small.[13,14] This phenomenon is often ascribed to ET from luminescent ions to vibrational modes of organic ligands or solvent molecules, which competes with radiative decay and thereby quenches the PL.[15−20] A common strategy to prevent such quenching is to grow a protective shell of undoped material around the NC core, shielding it from external influences.[13,16−20] An additional feature of doped NCs seems to be mostly overlooked: A donor ion close to the surface of a NC is likely to have fewer acceptor ions in its local environment,[21] so the probability for ET between the two species is lower. These finite-size effects will reduce the PL efficiency of NCs compared to bulk materials but have never been quantified, nor has the relevant size regime been identified.

Here, we investigate the impact of finite-size effects on ET in Tb^{3+},Yb^{3+} co-doped YPO_4 NCs. In bulk form, YPO_4:Tb^{3+},Yb^{3+} has previously been identified as a promising blue-to-near-infrared quantum-cutting phosphor for photovoltaics: Absorption of a single high-energy photon by a Tb^{3+} donor and subsequent ET to two Yb^{3+} acceptors lead to emission of two near-infrared photons that match the band gap of silicon. We measure the ET efficiency of the Tb^{3+} donor for NCs with different concentrations of Yb^{3+} acceptor ions and make a comparison with their previously investigated bulk counterparts.[4] The ET dynamics in nanocrystalline YPO_4:Tb^{3+},Yb^{3+} are markedly different. As donor ions close to the NC surface have fewer acceptor ions in proximity than donors in a bulk-like coordination, they have a lower rate of ET to acceptors and are less efficient quantum cutters. We demonstrate that this fundamental limitation on the ET efficiency can be

Received: September 21, 2021
Revised: October 30, 2021
Accepted: November 1, 2021
Published: November 8, 2021

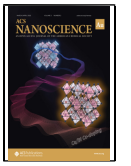

combated by suppressing the competitive pathway of radiative decay from Tb^{3+} donors in media with low refractive indices. Using these photonic effects,[22] we achieve high ET efficiencies despite the negative impact of the NC boundary. Our experimental results are supported by a Monte Carlo model that accounts for finite-size effects on the ET dynamics of Tb^{3+} donors in NCs. We identify the size range at which the ET efficiency in doped NCs is impacted by finite-size effects, which surprisingly includes NCs with diameters up to 12 nm. Our results are relevant in enabling rational design of efficient NC-based phosphor materials that rely on ET between a donor and an acceptor species.

RESULTS AND DISCUSSION

Quantum Cutting in YPO_4:Tb^{3+},Yb^{3+} NCs

We synthesized NCs of YPO_4 co-doped with Tb and Yb using the method by Oertel et al.[23] Based on transmission electron microscopy (Figure 1a), the NCs are anisotropic and appear similar in shape to the oblate octahedra reported for microcrystalline YPO_4.[24,25] The NCs have a long side of 8.1 ± 1.0 nm and a short/long axis ratio of 0.63 (Supporting Information). Upon excitation of Tb^{3+}, we observe PL both in the visible and near-infrared windows (Figure 1b). From experiments on bulk YPO_4, it is known that two competing pathways are responsible for the observed PL. On one hand, the $^5D_4$ level of Tb^{3+} decays by direct photon emission in the green−red. On the other hand, cooperative ET to two Yb^{3+} ions may occur—that is, Tb^{3+} acts as a donor and simultaneously transfers half of the excited-state energy to each Yb^{3+} acceptor—followed by photon emission in the near-infrared.[4]

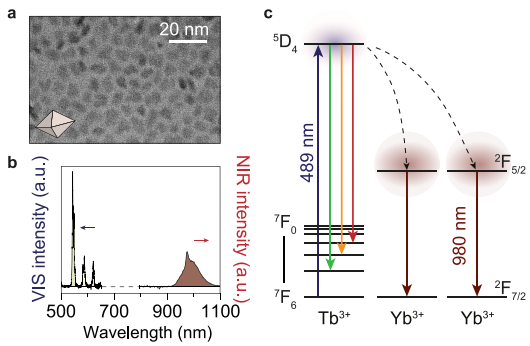

Figure 1. Quantum cutting in YPO_4:Tb^{3+},Yb^{3+} nanocrystals. (a) Transmission electron micrograph of octahedron-shaped YPO_4:Tb^{3+},Yb^{3+} nanocrystals. (b) Visible−near-infrared emission spectrum of $YbPO_4$ doped with 1% Tb^{3+} upon excitation in the $^5D_4$ level. (c) Energy level diagram: Upon excitation in the $^5D_4$ level of Tb^{3+} with blue light, cooperative energy transfer yields two excited Yb^{3+} ions that emit in the near-infrared.

We systematically measure the excited-state dynamics of the $^5D_4$ donor level for YPO_4 NCs doped with 1% Tb^{3+} and a range of Yb^{3+} concentrations. NCs doped solely with Tb^{3+} exhibit single-exponential decay with a rate of 0.31 ms^{-1} when dispersed in toluene (Figure 2a), typical for the rate of photon emission from the $^5D_4$ donor level.[4] By co-doping Yb^{3+} into the crystals (Figure 2b−e), we introduce the additional decay pathway of cooperative ET. The rate of cooperative ET from a donor to two nearby acceptors at distances r_A and r_B, respectively, scales as

$$\Gamma_{coop} = C_{coop} r_A^{-6} r_B^{-6} \quad (1)$$

where C_{coop} is a constant prefactor that we call the cooperative ET strength (previously determined to be 2.0×10^{-6} nm^{12} ms^{-1} for YPO_4:Tb^{3+},Yb^{3+}).[4,26] Assuming that dopants randomly occupy Y^{3+} lattice sites, the local coordination of a Tb^{3+} donor with Yb^{3+} acceptors is subject to statistical fluctuations. An ensemble of Tb^{3+} donors thus features a broad distribution of ET rates, giving rise to multiexponential decay.

The rate at which the $^5D_4$ level decays increases for higher concentrations of Yb^{3+} in our NCs, indicating that ET to acceptors becomes more dominant. Intuitively, we indeed expect that ET is faster when Tb^{3+} donors can transfer their excited-state energy to more acceptors. The total decay

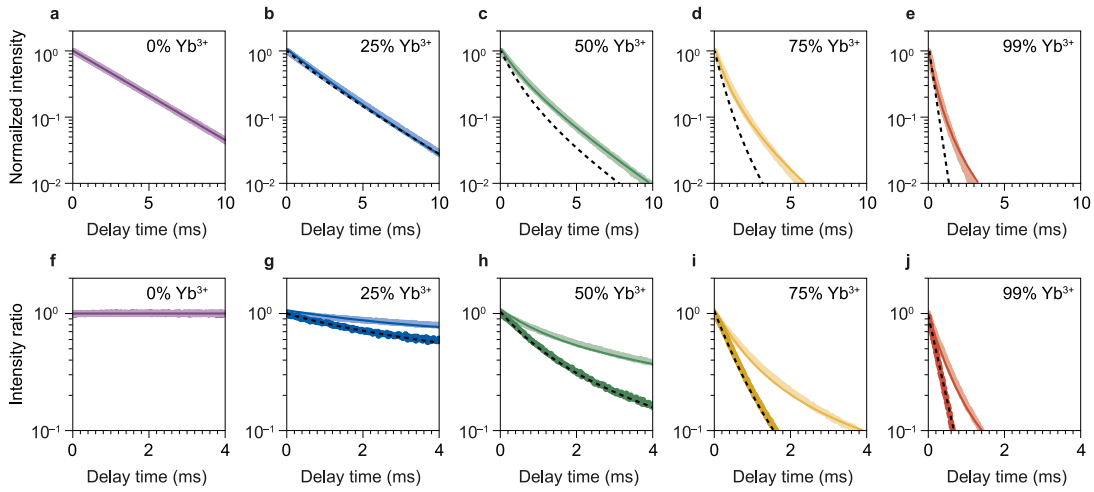

Figure 2. Excited-state dynamics of the Tb^{3+} $^5D_4$ level for NCs dispersed in toluene. (a−e) PL decay curves of YPO_4:Tb^{3+},Yb^{3+} with Yb^{3+} doping percentages of 0, 25, 50, 75 and 99%. Dashed lines are Monte Carlo simulations based on Tb^{3+} donors in a bulk-like coordination. Solid lines are fits to the Monte Carlo model based on Tb^{3+} donors randomly positioned in a nanocrystal with octahedral shape. (f−j) Contribution of ET to the decay dynamics, obtained by dividing the PL decay curves in (a−e) by the radiative decay in (a). Dark curves are the results for bulk YPO_4:Tb^{3+},Yb^{3+}, reproduced from a previous work of Vergeer et al.[4] The solid and dashed lines are the curves predicted by the Monte Carlo models for bulk and nanocrystalline YPO_4.

https://doi.org/10.1021/acsnanoscienceau.1c00033
ACS Nanosci. Au 2022, 2, 111−118

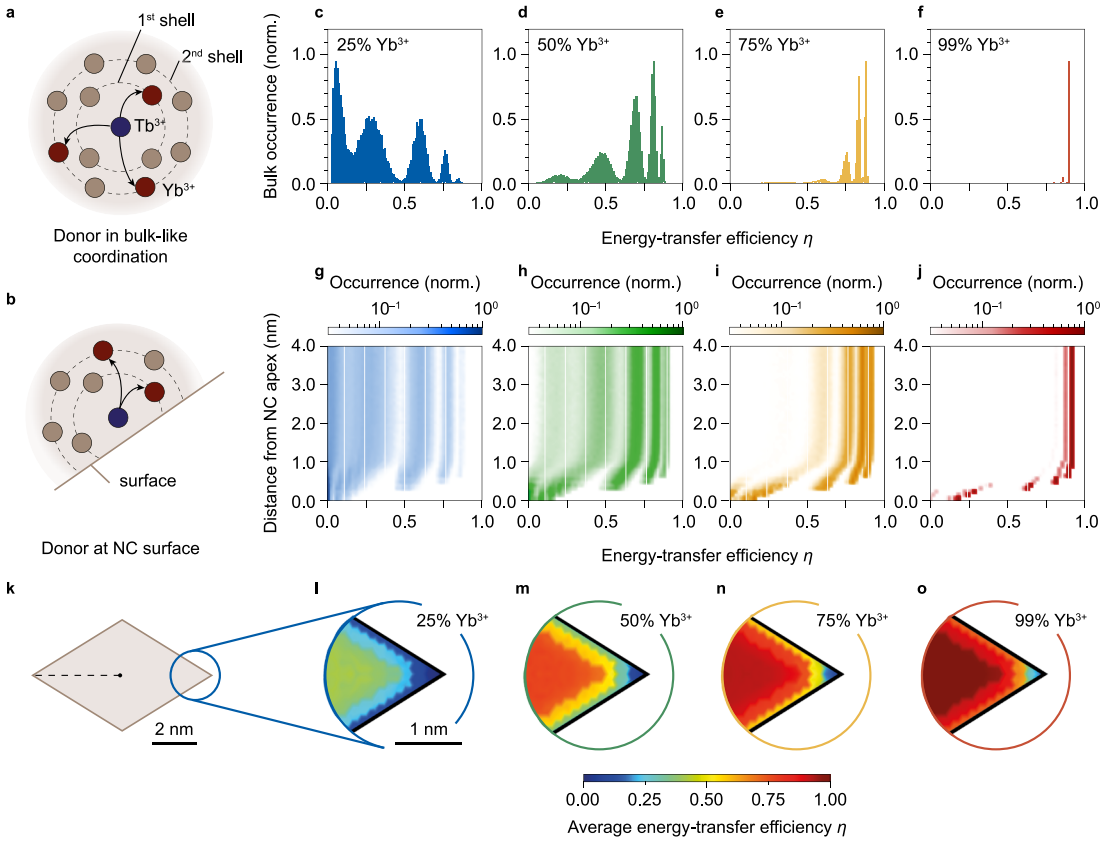

Figure 3. Results of Monte Carlo simulations of the energy transfer in YPO_4:Tb^{3+},Yb^{3+}. (a) A Tb^{3+} donor ion (blue) is surrounded by shells of nearest neighbors, next-nearest neighbors, etc. that consist of optically inactive Y^{3+} ions and Yb^{3+} acceptor ions. The exact distribution of Y^{3+} and Yb^{3+} ions is governed by the doping concentration. (b) Donor ions situated in proximity of the NC surface have incomplete shells and can accordingly transfer their energy to fewer acceptor ions. (c–f) Distribution of energy-transfer efficiencies η in bulk YPO_4:Tb^{3+},Yb^{3+} with doping percentages of 25, 50, 75, and 99%. (g–j) Distribution of energy-transfer efficiencies in nanocrystalline YPO_4:Tb^{3+},Yb^{3+} of octahedral shape, with different distances of the Tb^{3+} donor from the apex of the octahedron (the spatial coordinate on the vertical axis runs along the dashed line in (k), which shows a two-dimensional cross-cut of the octahedral nanocrystal). (l–o) Two-dimensional zoom-ins of (k), depicting in color scale how the distribution-averaged energy-transfer efficiency is governed by the position of the donor within the NC. In the above calculations, the surrounding medium is toluene.

dynamics of the Tb^{3+} PL due to the two competing pathways can be described as

$$I(t) = R(t)T(t) \tag{2}$$

where $R(t)$ is the contribution of radiative decay of Tb^{3+} and $T(t)$ is the decay resulting from cooperative ET to Yb^{3+}. To get a more direct measure of the ET dynamics, we extract the contribution of $T(t)$ by dividing the decay curves in Figure 2a–e by the single-exponential decay dynamics of Tb^{3+} in the absence of Yb^{3+}. The curves for the ET dynamics $T(t)$ are plotted in Figure 2f–j for different concentrations of Yb^{3+}. For the sake of comparison, the $T(t)$ curves for bulk YPO_4 are shown in the same panels (data reproduced from ref 4). The samples with Yb^{3+} all show multiexponential ET dynamics, reflecting contributions of the many Tb^{3+} centers with different rates of cooperative ET. Interestingly, the ET dynamics in NCs are markedly slower in comparison to their bulk counterpart (Figure 2f–j, dark curves). This, in turn, makes the efficiency of ET in NCs lower than in the bulk material.

We resort to theoretical modeling to understand the fundamental differences between ET in NCs and in bulk. Several models exist that describe ET dynamics between dopant ions in a host crystal. In crystalline host materials, acceptor ions can only occupy sites at discrete distances from the donor—that, is in shells of nearest neighbors, next-nearest neighbors, etc. While some models provide approximate expressions for the ET dynamics that ignore the discreteness of donor–acceptor spacings,[1,2] more dedicated models account for the crystal structure of the host material.[4,5,21,26,27] For instance, a donor ion in YPO_4 is coordinated by a shell of four nearest neighbors at a distance of 3.76 Å, four next-nearest-neighbors at 5.68 Å, and eight next-next-nearest neighbors at 5.72 Å.[28,29] To identify the mechanism of ET in bulk YPO_4:Tb^{3+},Yb^{3+}, Vergeer et al. used a Monte Carlo model based on the crystal parameters.[4] The Monte Carlo algorithm generated a multitude of random different donor environments from which the ensemble-averaged ET dynamics could be predicted. The experimental data for bulk YPO_4:Tb^{3+},Yb^{3+} were found to be in excellent agreement with a cooperative ET mechanism involving dipole–dipole coupling between a Tb^{3+} donor and two Yb^{3+} acceptors.[4] We compare the result of this previously used Monte Carlo model to our results on YPO_4:Tb^{3+},Yb^{3+} NCs (dashed lines in Figure 2b–e). It is immediately evident that the model does not capture the physics of ET in NCs, as the predicted decay is much faster than the experimental observations. More specifically, the decay dynamics of our NCs feature a range of donor environments with a rate of ET that is slower than

https://doi.org/10.1021/acsnanoscienceau.1c00033
ACS Nanosci. Au 2022, 2, 111–118

predicted. These donor environments must thus be coordinated by fewer Yb^{3+} acceptors, as expected for donor ions close to the surface of a NC.

We make an extension to the Monte Carlo model of Vergeer et al.[4] to account for finite-size effects experienced by donor ions in NCs. As microcrystalline YPO_4 is known to crystallize into oblate octahedra,[24,25] we assume that our NCs (Figure 1a) have a similar geometry. We model our NCs as oblate octahedra with a short half-axis of 2.5 nm and two long half-axes of 4 nm (Supporting Information and Figure S1). We take note that donor ions positioned close to the NC surface have fewer cation sites in their local environment available for Yb^{3+} acceptors (Figure 3a,b). Our extended Monte Carlo algorithm picks random positions for donor ions in the NC, accounts for the number of available cation sites around the donor, and then generates a random distribution of acceptor ions on these sites. As atomic details of surface faceting will vary between NCs in the experimental sample, we only take into account the discreteness of donor−acceptor distances but not the discreteness of donor positions within the NC. The Monte Carlo algorithm is further illustrated in the Supporting Information.

The solid lines in Figure 2 are results of simulations with our extended Monte Carlo algorithm. The decay curves predicted by our model for NCs have contributions of low ET rates and are in good quantitative agreement with the experimental observations. Minor deviations may be explained in terms of slight deviations in size and/or shape of the NCs in the experiments.

An important parameter that determines the quantum-cutting performance of our NCs is the ET efficiency. A high ET efficiency implies that incident blue photons are effectively converted into near-infrared excitations on Yb^{3+} while direct photon emission from Tb^{3+} in the visible window is minimal. The ET efficiency can be calculated from the decay dynamics using

$$\eta = 1 - \frac{\int R(t)\, T(t)\, \mathrm{d}t}{\int R(t)\, \mathrm{d}t} \tag{3}$$

Importantly, an ensemble of NCs is host to many different donor environments that each may have a different rate of ET and, as such, a different ET efficiency. The distributions of ET efficiencies for Tb donors in a bulk-like (thus, not accounting for finite-size effects) configuration are shown in Figure 3c−f for different concentrations of Yb^{3+} acceptors. The wide distributions in ET efficiency are due to the varying occupations of the neighbor shells in proximity of donors. The dominant factor determining the ET efficiency of a Tb^{3+} donor is the Yb^{3+} occupation number of the nearest-neighbor shell, which can have values of 0, 1, 2, 3, or 4 as is evident from the five peaks that are particularly clear in Figure 3d.

An important question is how exactly the ET efficiency of donors depends on their vicinity to the NC surface. To this end, we simulated the distribution of efficiencies for donors in the center of the NC (with a bulk-like environment) and those for donor sites closer to the surface. Distributions of the ET efficiency as a function of the distance from the apex of the octahedron (indicated by the dashed line in Figure 3k) are shown in the two-dimensional histograms in Figure 3g−j. While the distribution of ET efficiencies for donors in the center of a NC is very similar to the distribution in bulk YPO_4:Tb^{3+},Yb^{3+}, a shift to lower efficiencies is apparent for donor sites located within approximately 1 nm of the NC surface. Evidently, finite-size effects impose restrictions on the number of lattice sites close to a donor, which limits the acceptor occupancy and, therefore, the rate and efficiency of ET. Ultimately, donor ions confined to the NC apex have a vanishing ET efficiency as even the number of nearest-neighbor sites is restricted by finite-size effects. Maps of the average ET efficiency as a function of the spatial coordinate of the donor environment within the NC are shown in Figure 3l−o. The maps illustrate that, indeed, the average ET efficiency is substantially lower for donors close to the NC surface—particularly for those confined to the NC apex.

Photonic Effects as a Means to Tune ET Efficiency

For use in applications, reduced ET efficiencies due to finite-size effects are undesirable as they lead to lower output in the near-infrared. The ET efficiency is governed by a competition between two pathways: (1) direct emission of photons from the Tb^{3+} donor and (2) ET to Yb^{3+} acceptors. Previous work has shown that the ET rates depend solely on the distribution of acceptor ions around a central donor ion.[21] Therefore, it is impossible to accelerate ET between Tb^{3+} and Yb^{3+} using external factors. Interestingly, however, the radiative decay rate of the Tb^{3+} donor is tunable by changing the photonic environment of the NCs: The radiative rate is accelerated when NCs are embedded in media with a high refractive index, while low-index media slow down radiative decay.[21,22,30] Therefore, using photonic effects, it should be possible to control the competition between undesired radiative decay of Tb^{3+} and desired cooperative ET.

To test this effect, we systematically measured the PL decay dynamics of YPO_4:Tb^{3+},Yb^{3+} NCs dispersed in a range of solvents with different refractive indices (Supporting Information). Figure 4a shows the PL decay dynamics for NCs doped only with Tb^{3+}. The single-exponential decay of the $^5D_4$ level becomes faster upon changing the solvent from hexane to toluene and carbon disulfide, that is, increasing the refractive index n from 1.38 to 1.50 and 1.62,[31,32] respectively (Figure 4b). The decay rate measured previously on bulk YPO_4:Tb^{3+} (n = 1.75)[33] is even faster.[4] Assuming a unity quantum yield (QY) for bulk YPO_4:Tb^{3+} and allowing for a contribution of nonradiative decay in our NCs with a rate of 0.03 ms^{-1}, we find that our experimentally measured decay rates are in excellent agreement with the NC-cavity model for ellipsoidal NCs (Supporting Information).[22,34] Such a contribution of nonradiative decay present only in NCs is likely due to some quenching of Tb^{3+} by surface defects or ligands and has been reported previously.[22]

Figure 4c shows ET efficiencies as obtained using eq 3. The functions $R(t)$ are extracted from experimental results, and $T(t)$ are either obtained from experimental results or calculated with our Monte Carlo model. The results for bulk YPO_4:Tb^{3+},Yb^{3+} are based on the experimental data obtained by Vergeer et al.[4] (solid lines). The experimental efficiencies are slightly lower than those predicted by the Monte Carlo model (dashed lines), possibly due to a contribution of nonradiative relaxation. Filled bars indicate the ET efficiencies measured for NCs embedded in different solvents, while the open bars are the results of our Monte Carlo simulations including finite-size effects. Again, the experimental efficiencies are somewhat lower than those predicted by the model, which is likely due to nonradiative relaxation pathways. Nevertheless, our experiments and model both show that the ET efficiency is

https://doi.org/10.1021/acsnanoscienceau.1c00033
ACS Nanosci. Au 2022, 2, 111−118

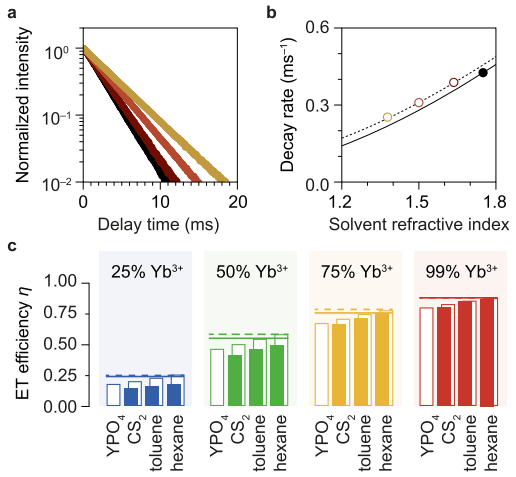

Figure 4. Photonic effects on the radiative decay rate of the donor impact the energy-transfer efficiency. (a) PL decay curves of the $^5D_4$ level of Tb^{3+} for NCs dispersed in hexane, toluene, CS_2, and bulk YPO_4:Tb^{3+}(1%) (refractive indices n = 1.38, 1.50, 1.62, and 1.75, respectively; increasingly dark colors). (b) Dependence of the $^5D_4$ radiative rate on the refractive index of the medium (open circles, NCs dispersed in different solvents; filled circle, bulk YPO_4:Tb^{3+}).[4] The solid line is the prediction of the NC-cavity model for ellipsoidal NCs with a QY of 1.0, while the dashed line contains a contribution of nonradiative decay rate of 0.3 ms^{-1}. (c) ET efficiencies of NCs dispersed in different environments. Filled bars are the ET efficiencies measured experimentally. Open bars are Monte Carlo calculations for NCs in media with different refractive indices (YPO_4 denotes an YPO_4:Tb^{3+},Yb^{3+} NC, including finite-size effects on ET, surrounded by a region of undoped YPO_4). Solid lines are the ET efficiencies of bulk YPO_4:Tb^{3+}(1%),Yb^{3+}(x%) obtained experimentally,[4] and dashed lines are Monte Carlo calculations.

highest when the NCs are dispersed in low-index solvents, such as hexane.

It is instructive to compare the result of our Monte Carlo calculations for bulk YPO_4:Tb^{3+},Yb^{3+} (dashed lines) to those for NCs embedded in an environment with refractive index n = 1.75, similar to that of the YPO_4 host material (leftmost open bars). This comparison highlights the finite-size effects on the ET efficiency without any photonic influences. The ET efficiency for NCs in an environment with n = 1.75 is lower than that of bulk YPO_4:Tb^{3+},Yb^{3+} by 10−30% relative, with the biggest decrease for low Yb^{3+} acceptor concentrations. Interestingly, however, this negative effect can be compensated for when the NCs are embedded in solvents with low refractive indices. We thus demonstrate that by controlling the photonic environment of our NCs, we can control the balance between ET from the donor and direct emission from the donor level.

At What Dimensions Do Finite-Size Effects Play a Role?

In the following, we will investigate, using theory and simulations, at what NC sizes one should consider finite-size effects on the efficiency of ET between dopants. While our foregoing discussion focused on cooperative ET between a Tb^{3+} donor and two Yb^{3+} acceptors, here, we broaden the scope and also consider the most common ET mechanism: first-order ET of the Förster type, i.e., dipole−dipole coupling between a single donor and a single acceptor. We note that other mechanisms of ET with different distance dependencies may occur in some phosphors,[6,35] but we limit our discussion on finite-size effects to ET via the mechanism of dipole−dipole coupling. As examples, we use experimentally determined rate constants for cooperative ET between Tb^{3+} and Yb^{3+} in YPO_4 (k_{rad} = 1/(2.3 ms), C_{coop} = 2.0 × 10^{-6} nm^{12} ms^{-1})[4] and the first-order (cross-relaxation) ET process between Pr^{3+} and Yb^{3+} in $LiYF_4$ (k_{rad} = 1/(35 μs), C_{et} = 2 × 10^{-3} nm^6 μs^{-1}).[5] We apply our Monte Carlo algorithm to calculate the average ET efficiency η in simple spherical NCs as a function of the NC radius. Figure 5a,c shows the resulting efficiencies normalized

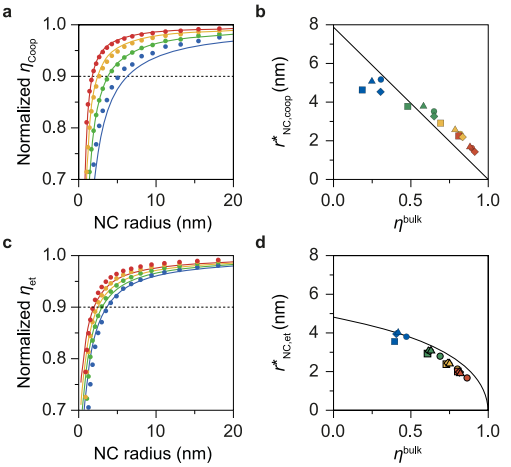

Figure 5. Finite-size effects on the ET efficiency of nanocrystalline phosphors. (a) Cooperative ET efficiencies in spherical NCs normalized to the efficiencies of their bulk counterparts, for the Tb^{3+}−Yb^{3+} couple in YPO_4 with Yb^{3+} concentrations of 25, 50, 75, and 99% (blue, green, yellow, and red). Solid lines are the predictions of our simplified analytical model (Supporting Information), and full circles are the results of Monte Carlo calculations. (b) Critical NC radii as a function of the bulk ET efficiency for cooperative ET in the lattices of $LaPO_4$, YPO_4, β-$NaYF_4$, and BaF_2 (squares, triangles, diamonds, and circles, respectively). We use the rate parameters k_{rad} = 1/(2.3 ms) and C_{coop} = 2.0 × 10^{-6} nm^{12} ms^{-1}, which were determined experimentally for YPO4:Tb^{3+},Yb^{3+}. The black solid line is the result of eq 4. (c, d) Same as (a) and (b) but for first-order ET, using the rate parameters k_{rad} = 1/(35 μs) and C_{et} = 2 × 10^{-3} nm^6 μs^{-1} from the Pr^{3+}−Yb^{3+} couple in $LiYF_4$. In (c), we consider YPO_4:Pr^{3+} with Yb^{3+} acceptor concentrations of 2.5, 5.0, 7.5, and 10% (blue, green, yellow, and red). The black solid line in (d) is the result of eq 5.

to the bulk ET efficiency η^{bulk}. We see that the ET efficiencies drop by 10% compared to η^{bulk} at a NC radius of 2−6 nm, depending on the doping concentration, for cooperative as well as first-order ET. These significant finite-size effects are consistent with the observation of a 10−30% finite-size effect on cooperative ET in anisotropic YPO_4:Tb^{3+},Yb^{3+} NCs of approximately 8 by 5 nm (full length). We find that finite-size effects in NCs are more pronounced when the corresponding bulk phosphor has a low ET efficiency (that is, the ET efficiency drops more rapidly with decreasing NC radius). This is also evident from Figure 4, and we can understand this because phosphors with low bulk ET efficiencies rely more strongly on long-range interactions and are thus more strongly affected by finite-size effects (Supporting Information).

To quantify at what length scale finite-size effects become non-negligible, we define the critical NC radius r_{NC}* where the ET efficiency has dropped by 10% relative to that of the bulk phosphor with the same concentrations of acceptor ions. We calculated the critical radii for cooperative ET between Tb^{3+} and Yb^{3+} as well as for first-order ET between Pr^{3+} and Yb^{3+}. To investigate a possible effect of the nature of the host crystal, we place these ions in different crystalline environments by

https://doi.org/10.1021/acsnanoscienceau.1c00033
ACS Nanosci. Au 2022, 2, 111−118

substitutional doping while keeping k_{rad}, C_{coop}, and C_{et} the same. We consider YPO_4, $LaPO_4$, β-$NaYF_4$, and BaF_2, which are different in terms of crystal symmetry, density of lattice sites at which the acceptor ions can substitute, number of nearest-neighbor sites, and nearest-neighbor distance. More precisely, these four crystals have rare-earth site densities of ρ = 14.0, 13.0, 13.8, and 16.8 nm^{-3}, number of nearest-neighbor sites N = 4, 2, 2, and 12, and nearest-neighbor distances of 0.38, 0.41, 0.35, and 0.44 nm, respectively.[29,36−38] Figure 5b,d shows the critical radii for the Tb^{3+}−Yb^{3+} and Pr^{3+}−Yb^{3+} pairs in the different crystalline environments and with different concentrations of acceptor ions. Surprisingly, the impact of the crystal structure of the host material is only marginal (note that all data points of the same color are close together in Figure 5b,d), even though this strongly impacts the arrangement of acceptor ions around a donor ion. Instead, the critical radius of nanocrystalline phosphors appears to be governed by the ET efficiency of the corresponding bulk phosphor.

While our Monte Carlo model captures the most important features of ET in nanocrystalline phosphors, it is computationally expensive and complex to implement. It is therefore desirable to have a simpler model that nonetheless provides a good estimate of the critical NC radius. We introduce simple analytical models for first-order ET and cooperative ET (Supporting Information) that assume a homogeneous distribution of acceptor ions over the volume of the NC and neglect the discreteness of donor−acceptor spacings in a crystalline environment. Despite these simplifications, the resulting analytical expressions are a good prediction for finite-size effects (Figure 5a,c). Moreover, the models provide simple and general expressions for the critical NC radius. For cooperative ET, the critical NC radius is given by

$$r^*_{NC,coop} = \frac{5}{2} r_{min}(1 - \eta^{bulk}_{coop}) \tag{4}$$

where r_{min} is the minimum distance between donors and acceptors in the analytical model (approximately equal to the nearest-neighbor distance in the crystal, with typical values of 0.35−0.4 nm). For first-order ET, the expression for the critical NC radius is

$$r^*_{NC,et} = -\frac{20}{3} R_0 \left\{ \sqrt{1 - \eta^{bulk}_{et}} + (1 - \eta^{bulk}_{et}) \left[\frac{1}{2} \ln(1 - \eta^{bulk}_{et}) - 1 \right] \right\} \Big/ [\eta^{bulk}_{et} \ln(1 - \eta^{bulk}_{et})] \tag{5}$$

with R_0 being the Förster radius, which is defined as $R_0 = (C_{et} / k_{rad})^{1/6}$. The results of eqs 4 and 5are shown as solid lines in Figure 5b,d. Interestingly, the critical NC radius depends on the optical properties of the donor−acceptor pair or the acceptor concentration only indirectly through the bulk ET efficiency η^{bulk}. It is clear that, although finite-size effects may be small for phosphors with a high η^{bulk}, critical radii are as big as 6 nm for low values of η^{bulk}. This suggests that finite-size effects may pose a challenge in the development of various applications that rely on ET and where small NCs are a requirement. For instance, quantum-cutting phosphors most effectively enhance the efficiency of photovoltaic energy conversion when scattering losses are minimized, thus necessitating small particles. Alternatively, small sizes may be essential to use lanthanide-doped NCs as fluorescent probes for high-resolution (in vivo) imaging or sensing.[9,16,39] Furthermore, many phosphor materials are synthesized with dimensions in the critical size regime even though there is no stringent requirement for small NC sizes.[40,41] The significant finite-size effects on ET experimentally demonstrated in Figure 4 and calculated in Figure 5 are thus important for many nanocrystalline phosphor materials and may occur for any donor−acceptor combination and in any host crystal.

CONCLUSIONS

We have presented a study on the excited-state decay dynamics of the Tb^{3+} $^5D_4$ donor level in bulk and nanocrystalline YPO_4:Tb^{3+},Yb^{3+} quantum-cutting phosphors to provide insight to the role of finite-size effects on the ET efficiency in nanocrystals. The decay dynamics result from a competition between direct emission of photons in the visible window on one hand and ET to Yb^{3+} acceptors on the other. We analyzed the dynamics of ET by systematic measurements for different concentrations of acceptor ions and found that compared to bulk, ET dynamics are markedly slower in nanocrystalline phosphors. We presented a simple Monte Carlo model that randomly simulates many possible environments of a central Tb^{3+} donor ion in terms of both the distribution of Yb^{3+} acceptors and the position within the nanocrystal. The model explains the reduced ET rate in NCs as a result of finite-size effects: Tb^{3+} donors located close to the NC surface have on average fewer Yb^{3+} acceptors in proximity and, thus, a lower ET efficiency. Although it is not possible to accelerate ET by external factors, the competing pathway of photon emission from the Tb^{3+} donor level can be suppressed. Tuning the photonic environment of the NCs by embedding them in an environment with a low refractive index slows down the radiative decay of Tb^{3+}. Using this method, we are able to compensate for the negative impact of finite-size effects on the ET efficiency and, in fact, achieve ET efficiencies in nanocrystalline YPO_4:Tb^{3+},Yb^{3+} that are as high as those of the bulk material. We provide general rules for the critical length scale at which finite-size effects reduce ET efficiencies in NCs. Importantly, while the performance of ultrasmall nanocrystalline phosphors may be improved by controlling undesirable quenching mechanisms related to chemical species at the NC surface, finite-size effects on ET between dopants pose a fundamental limitation that can only be opposed by tuning the photonic environment.

METHODS

Synthesis and Characterization of Doped YPO_4 NCs

Chemicals used include yttrium chloride (99.99%, Sigma-Aldrich), terbium chloride (99.99%, Sigma-Aldrich), ytterbium chloride (99.99%, Sigma-Aldrich), methanol (99.6%, Sigma-Aldrich), tributyl phosphate (≥99%, Sigma-Aldrich), diphenyl ether (≥98%, Sigma-Aldrich), tributyl amine (≥98.5%, Sigma-Aldrich), phosphoric acid (≥99%, Sigma-Aldrich), dihexyl ether (97%, Sigma-Aldrich), dodecylamine (98%, Sigma-Aldrich), toluene (99.9%, Sigma-Aldrich), hexane (99%, Sigma-Aldrich), and carbon disulfide (≥99%, Sigma-Aldrich). All chemicals were used without further purification unless specified otherwise.

NCs were synthesized using the method of Oertel et al.[23] Briefly, a clear solution of 10 mmol of rare-earth chlorides (Y, Tb, Tb) in 10 mL of methanol was mixed with 11 mL of tributyl phosphate. Methanol was evaporated under vacuum at room temperature, after which 30 mL of diphenyl ether was added. Following the removal of water under vacuum at 105 °C, 40 mmol of tributylamine and 7 mL of a 2 M solution of phosphoric acid in dihexyl ether were added. Subsequently, the reaction mixture was kept overnight under nitrogen

https://doi.org/10.1021/acsnanoscienceau.1c00033
ACS Nanosci. Au 2022, 2, 111−118

at 200 °C, during which the NCs were formed. Ligand exchange was performed by the addition of 50 mL of dodecylamine. After an additional 3 h at 200 °C and cooling down to room temperature, the supernatant was discarded following centrifugation (10 min at 800*g*) and the residue was redispersed in 10 mL of toluene, washed with 15 mL of methanol, and centrifuged again. The residue was dried under a vacuum. NCs were dispersed in hexane, toluene, or carbon disulfide for different measurements.

Photoluminescence Measurements

PL spectra were measured using an Edinburgh Instruments FLS920 fluorescence spectrometer equipped with a Hamamatsu R928 photomultiplier tube for the visible range and a liquid nitrogen-cooled Hamamatsu R5509 photomultiplier tube for the near-infrared range. Tb^{3+} ions were excited using the third harmonic of a Nd:YAG laser at 355 nm with a repetition rate of 20 Hz. The PL decay curve of the $^5D_4$ level was obtained by pulsed excitation with an Ekspla NT342B laser at 488.8 nm at a repetition rate of 10 Hz. The emission at 545 nm was detected using a Triax 550 monochromator and Hamamatsu H7422-02 photomultiplier tube coupled to a PicoQuant TimeHarp 260 photon counting module.

■ ASSOCIATED CONTENT

Supporting Information

The Supporting Information is available free of charge at https://pubs.acs.org/doi/10.1021/acsnanoscienceau.1c00033.

Further details related to the Monte Carlo model analytical models and additional background on photonic effects (PDF)

■ AUTHOR INFORMATION

Corresponding Author

Freddy T. Rabouw − *Debye Institute for Nanomaterials Science, Utrecht University, 3584 CC Utrecht, The Netherlands;* orcid.org/0000-0002-4775-0859; Email: f.t.rabouw@uu.nl

Authors

Mark J. J. Mangnus − *Debye Institute for Nanomaterials Science, Utrecht University, 3584 CC Utrecht, The Netherlands;* orcid.org/0000-0002-3595-8097

Jeffrey Zom − *Debye Institute for Nanomaterials Science, Utrecht University, 3584 CC Utrecht, The Netherlands*

Tom A. J. Welling − *Debye Institute for Nanomaterials Science, Utrecht University, 3584 CC Utrecht, The Netherlands*

Andries Meijerink − *Debye Institute for Nanomaterials Science, Utrecht University, 3584 CC Utrecht, The Netherlands;* orcid.org/0000-0003-3573-9289

Complete contact information is available at: https://pubs.acs.org/10.1021/acsnanoscienceau.1c00033

Author Contributions

The manuscript was written through contributions of all authors. All authors have given approval to the final version of the manuscript.

Notes

The authors declare no competing financial interest.

■ ACKNOWLEDGMENTS

This work was supported by The Netherlands Center for Multiscale Catalytic Energy Conversion (MCEC), an NWO Gravitation Programme funded by the Ministry of Education, Culture, and Science of the government of The Netherlands.

■ REFERENCES

(1) Inokuti, M.; Hirayama, F. Influence of Energy Transfer by the Exchange Mechanism on Donor Luminescence. *J. Chem. Phys.* **1965**, *43*, 1978−1989.

(2) Yokota, M.; Tanimoto, O. Effects of Diffusion on Energy Transfer by Resonance. *J. Phys. Soc. Jpn.* **1967**, *22*, 779−784.

(3) Auzel, F. Upconversion and Anti-Stokes Processes with f and d Ions in Solids. *Chem. Rev.* **2004**, *104*, 139−174.

(4) Vergeer, P.; Vlugt, T. J. H.; Kox, M. H. F.; den Hertog, M. I.; van der Eerden, J. P. J. M.; Meijerink, A. Quantum Cutting by Cooperative Energy Transfer in $Yb_xY_{1-x}PO_4$: Tb^{3+}. *Phys. Rev. B* **2005**, *71*, No. 014119.

(5) van Wijngaarden, J. T.; Scheidelaar, S.; Vlugt, T. J. H.; Reid, M. F.; Meijerink, A. Energy Transfer Mechanism for Downconversion in the (Pr^{3+}, Yb^{3+}) Couple. *Phys. Rev. B* **2010**, *81*, 155112.

(6) Yu, D. C.; Rabouw, F. T.; Boon, W. Q.; Kieboom, T.; Ye, S.; Zhang, Q. Y.; Meijerink, A. Insights into the Energy Transfer Mechanism in Ce^{3+}-Yb^{3+} Codoped YAG Phosphors. *Phys. Rev. B* **2020**, *9*, 165126.

(7) Brites, C. D. S.; Lima, P. P.; Silva, N. J. O.; Millán, A.; Amaral, V. S.; Palacio, F.; Carlos, L. D. Thermometry at the Nanoscale. *Nanoscale* **2012**, *4*, 4799−4829.

(8) Jaque, D.; Vetrone, F. Luminescence Nanothermometry. *Nanoscale* **2012**, *4*, 4301−4326.

(9) van Swieten, T. P.; van Omme, T.; van den Heuvel, D. J.; Vonk, S. J. W.; Spruit, R. G.; Meirer, F.; Pérez Garza, H. H.; Weckhuysen, B. M.; Meijerink, A.; Rabouw, F. T.; Geitenbeek, R. G. Mapping Elevated Temperatures with a Micrometer Resolution Using the Luminescence of Chemically Stable Upconversion Nanocrystals. *ACS Appl. Nano Mater.* **2021**, *4*, 4208−4215.

(10) Zhou, B.; Shi, B.; Jin, D.; Liu, X. Controlling Upconversion Nanocrystals for Emerging Applications. *Nature Nanotech.* **2015**, *10*, 924−936.

(11) Li, H.; Wang, X.; Ohulchanskyy, T. Y.; Chen, G. Lanthanide-Doped Near-Infrared Nanoparticles for Biophotonics. *Adv. Mater.* **2021**, *33*, 2000678.

(12) van der Ende, B. M.; Aarts, L.; Meijerink, A. Lanthanide Ions as Spectral Converters for Solar Cells. *Phys. Chem. Chem. Phys.* **2009**, *11*, 11081−11095.

(13) Wang, F.; Wang, J.; Liu, X. Direct Evidence of a Surface Quenching Effect on Size-Dependent Luminescence of Upconversion Nanoparticles. *Angew. Chem., Int. Ed.* **2010**, *49*, 7456−7460.

(14) Zhao, J.; Lu, Z.; Yin, Y.; McRae, C.; Piper, J. A.; Dawes, J. M.; Jin, D.; Goldys, E. M. Upconversion Luminescence with Tunable Lifetime in $NaYF_4$:Yb,Er Nanocrystals: Role of Nanocrystal Size. *Nanoscale* **2013**, *5*, 944−952.

(15) Stouwdam, J. W.; Hebbink, G. A.; Huskens, J.; van Veggel, F. C. J. M. Lanthanide-Doped Nanoparticles with Excellent Luminescent Properties in Organic Media. *Chem. Mater.* **2003**, *15*, 4604−4616.

(16) Gargas, D. J.; Chan, E. M.; Ostrowski, A. D.; Aloni, S.; Altoe, M. V. P.; Barnard, E. S.; Sanii, B.; Urban, J. J.; Milliron, D. J.; Cohen, B. E.; Schuck, P. J. Engineering Bright Sub-10-nm Upconverting Nanocrystals for Single-Molecule Imaging. *Nat. Nanotechnol.* **2014**, *9*, 300−305.

(17) Fischer, S.; Johnson, N. J. J.; Pichaandi, J.; Goldschmidt, J. C.; van Veggel, F. C. J. M. Upconverting Core-Shell Nanocrystals with High Quantum Yield under Low Irradiance: On the Role of Isotropic and Thick Shells. *J. Appl. Phys.* **2015**, *118*, 193105.

(18) Fischer, S.; Bronstein, N. D.; Swabeck, J. K.; Chan, E. M.; Alivisatos, A. P. Precise Tuning of Surface Quenching for Luminescence Enhancement in Core−Shell Lanthanide-Doped Nanocrystals. *Nano Lett.* **2016**, *16*, 7241−7247.

(19) Rabouw, F. T.; Prins, P. T.; Villaneuva-Delgado, P.; Castelijns, M.; Geitenbeek, R. G.; Meijerink, A. Quenching Pathways in $NaYF_4$:Er^{3+},Yb^{3+} Upconversion Nanocrystals. *ACS Nano* **2018**, *12*, 4812−4823.

(20) Homann, C.; Krukewitt, L.; Frenzel, F.; Grauel, B.; Würth, C.; Resch-Genger, U.; Haase, M. $NaYF_4$:Yb,Er/$NaYF_4$ Core/Shell Nanocrystals with High Upconversion Luminescence Quantum Yield. *Angew. Chem., Int. Ed.* **2018**, *57*, 8765−8769.
(21) Rabouw, F. T.; den Hartog, S. A.; Senden, T.; Meijerink, A. Photonic Effects on the Förster Resonance Energy Transfer Efficiency. *Nat. Commun.* **2014**, *5*, 3610.
(22) Senden, T.; Rabouw, F. T.; Meijerink, A. Photonic Effects on the Radiative Decay Rate and Luminescence Quantum Yield of Doped Nanocrystals. *ACS Nano* **2015**, *9*, 1801−1808.
(23) Oertel, A.; Lengler, C.; Walther, T.; Haase, M. Photonic Properties of Inverse Opals Fabricated from Lathanide-Doped $LaPO_4$ Nanocrystals. *Chem. Mater.* **2009**, *21*, 3883−3888.
(24) Guan, H.; Lv, C.; Han, C.; Zhu, D. Luminescent and Magnetism Properties of YPO_4:Eu^{3+} Octahedron Microcrystals. *Mater. Lett.* **2012**, *81*, 92−94.
(25) Shao, B.; Feng, Y.; Zhao, S.; Yuan, S.; Huo, J.; Lü, W.; You, H. Phase-Tunable Synthesis of Monodisperse YPO_4:Ln^{3+} (Ln = Ce, Eu, Tb) Micro/Nanocrystals via Topotactic Transformation Route with Multicolor Luminescence Properties. *Inorg. Chem.* **2017**, *56*, 6114−6121.
(26) Rabouw, F. T.; Meijerink, A. Modeling the Cooperative Energy Transfer Dynamics of Quantum Cutting for Solar Cells. *J. Phys. Chem. C* **2015**, *119*, 2364−2370.
(27) Siebold, H.; Heber, J. "Discrete Shell Model" for Analysing Time-Resolved Energy Transfer in Solids. *J. Lumin.* **1981**, *22*, 297−319.
(28) Milligan, W. O.; Mullica, D. F.; Beall, G. W.; Boatner, L. A. Structural Investigations of YPO_4, $ScPO_4$, and $LuPO_4$. *Inorg. Chim. Acta* **1982**, *60*, 39−43.
(29) Ni, Y.; Hughes, J. M.; Mariano, A. N. Crystal Chemistry of the Monazite and Xenotime Structures. *Am. Mineral.* **1995**, *80*, 21−26.
(30) Meltzer, R. S.; Feofilov, S. P.; Tissue, B.; Yuan, H. B. Dependence of Fluorescence Lifetimes of Y_2O_3:Eu^{3+} Nanoparticles on the Surrounding Medium. *Phys. Rev. B* **1999**, *60*, R14012−R14015.
(31) Kozma, I. Z.; Krok, P.; Riedle, E. Direct Measurement of the Group-Velocity Mismatch and Derivation of the Refractive-Index Dispersion for a Variety of Solvents in the Ultraviolet. *J. Opt. Soc. Am. B* **2005**, *22*, 1479−1485.
(32) Kedenburg, S.; Vieweg, M.; Gissibl, T.; Giessen, H. Linear Refractive Index and Absorption Measurements of Nonlinear Optical Liquids in the Visible and Near-Infrared Spectral Region. *Opt. Mater. Express* **2012**, *2*, 1588−1611.
(33) Jellison, G. E., Jr.; Boatner, L. A.; Chen, C. Spectroscopic Refractive Indices of Metalorthophosphates with the Zircon-type Structure. *Opt. Mater.* **2000**, *15*, 103−109.
(34) Toptygin, D. Effects of the Solvent Refractive Index and its Dispersion on the Radiative Decay Rate and Extinction Coefficient of a Fluorescent Solute. *J. Fluoresc.* **2003**, *13*, 201−219.
(35) Malta, O. L. Mechanisms of Non-Radiative Energy Transfer Involving Lanthanide Ions Revisited. *J. Non-Cryst. Solids* **2008**, *354*, 4770−4776.
(36) Wyckoff, R. W. G. Fluorite Structure. In *Crystal Structures 1*; 2nd ed., Interscience Publishers: New York, 1963, pp. 239−444
(37) Villanueva-Delgado, P.; Krämer, K. W.; Valiente, R. Simulating Energy Transfer and Upconversion in β-$NaYF_4$: Yb^{3+}, Tm^{3+}. *J. Phys. Chem. C* **2015**, *119*, 23648−23657.
(38) Aebischer, A.; Hostettler, M.; Hauser, J.; Krämer, K.; Weber, T.; Güdel, H. U.; Bürgi, H. B. Structural and Spectroscopic Characterization of Active Sites in a Family of Light-Emitting Sodium Lanthanide Tetrafluorides. *Angew. Chem., Int. Ed.* **2006**, *45*, 2802−2806.
(39) Liu, Q.; Sun, Y.; Yang, T.; Feng, W.; Li, C.; Li, F. Sub-10 nm Hexagonal Lanthanide-Doped $NaLuF_4$ Upconversion Nanocrystals for Sensitive Bioimaging in Vivo. *J. Am. Chem. Soc.* **2011**, *133*, 17122−17125.
(40) Wang, F.; Lin, X. Recent Advances in the Chemistry of Lanthanide-Doped Upconversion Nanocrystals. *Chem. Soc. Rev.* **2009**, *38*, 976−989.
(41) Wang, G.; Peng, Q.; Li, Y. Lanthanide-Doped Nanocrystals: Synthesis, Optical-Magnetic Properties, and Applications. *Acc. Chem. Res.* **2011**, *44*, 322−332.

https://doi.org/10.1021/acsnanoscienceau.1c00033
ACS Nanosci. Au 2022, 2, 111−118